J. Fluid Mech. (2012), *vol.* 712, *pp.* 273–294.
doi:10.1017/jfm.2012.418

Multiple equilibria in a simple elastocapillary system

Michele Taroni[1] **and Dominic Vella**[1,2]†

[1] Oxford Centre for Collaborative Applied Mathematics, Mathematical Institute, 24-29 St Giles', Oxford OX1 3LB, UK

[2] Department of Applied Mathematics and Theoretical Physics, University of Cambridge, Wilberforce Rd, Cambridge CB3 0WA, UK

(Received 11 February 2012; revised 31 May 2012; accepted 16 August 2012; first published online 28 September 2012)

We consider the elastocapillary interaction of a liquid drop placed between two elastic beams, which are both clamped at one end to a rigid substrate. This is a simple model system relevant to the problem of surface-tension-induced collapse of flexible microchannels that has been observed in the manufacture of microelectromechanical systems (MEMS). We determine the conditions under which the beams remain separated, touch at a point, or stick along a portion of their length. Surprisingly, we show that in many circumstances multiple equilibrium states are possible. We develop a lubrication-type model for the flow of liquid out of equilibrium and thereby investigate the stability of the multiple equilibria. We demonstrate that for given material properties two stable equilibria may exist, and show via numerical solutions of the dynamic model that it is the initial state of the system that determines which stable equilibrium is ultimately reached.

Key words: capillary flows, lubrication theory, MEMS/NEMS

1. Introduction

Recently, there has been great interest in the interaction between elastic and capillary forces, commonly referred to as 'elastocapillarity' (Roman & Bico 2010). While this activity has primarily been driven by applications at the microscopic scale (where objects are often sufficiently flexible that surface forces are strong enough to bend them) there are also a number of everyday situations in which elastocapillary effects can be observed. For example, the bending of paintbrush hairs caused by wetting with a liquid motivated several experiments to investigate the elastocapillary analogue of capillary rise (Bico *et al.* 2004; Kim & Mahadevan 2006). In a similar vein, though not visible to the naked eye, the closure of airways within the lung is controlled by the interaction between elasticity and the surface tension of the liquid lining of the airway (Grotberg & Jensen 2004).

The possibility of elastic deformation in response to capillary forces is important for understanding the force balance at a contact line; while Young's law relating surface energies and the equilibrium contact angle was derived from a tangential force balance more than two centuries ago (Young 1805), the corresponding normal force balance is more controversial. In this regard, variational principles have been used to determine

† Email address for correspondence: dominic.vella@cantab.net

the correct boundary conditions for specific equilibrium elastocapillary problems with given surface energies (see Shanahan 1985, for example). These conditions resolve how the liquid behaves in response to the deformation of the solid and show that there is a small modification to the equilibrium contact angle as a result of the elastic deformation. However, more recent calculations appear to show the presence of an unexpected tangential force on the solid of the same order as the normal force (and hence not negligible) (Das *et al.* 2011; Marchand *et al.* 2012).

Controversy aside, the static balance between elastic and capillary forces has been applied to a broad range of problems, including the statistics of aggregation between the many bristles of a wet brush (Boudaoud, Bico & Roman 2007), the spontaneous wrapping of a droplet with an elastic sheet (so-called 'capillary origami': Py *et al.* 2007), the capillary-induced wrinkling of a thin sheet (Huang *et al.* 2007; Vella, Adda-Bedia & Cerda 2010), and the wrapping of a flat sheet onto a sticky surface (Hure, Roman & Bico 2011).

More recently attention has shifted to understanding the fluid motions that occur in such problems. Early work focused on situations in which the bending stiffness of the sheet could be neglected in favour of a known membrane tension: for reviews see Grotberg & Jensen (2004) and Craster & Matar (2009). This coupling between thin-film fluid flows, surface tension and a membrane under tension is relevant to instabilities in the liquid lining of the lungs (Halpern & Grotberg 1992) or in the creation of textured surfaces (Matar & Kumar 2004). Studies incorporating bending stiffness (but invariably neglecting tension) have tended to study surface-tension-driven rise between two elastic beams. In the presence of gravity, so-called 'elastocapillary rise', a finite rise height is reached (Duprat, Aristoff & Stone 2011). In the absence of gravity the liquid meniscus continues to move until it reaches the edge of the system; such motion has been studied by van Honschoten *et al.* (2007) and Aristoff, Duprat & Stone (2011).

The present study is motivated by the fabrication of microelectromechanical systems (MEMS), which frequently involves the interaction between the surface tension of a solvent and the elasticity of the components of a MEMS device. This can happen either in the fabrication of a 'mask' using photolithography (Berkowski *et al.* 2005) or in the stamping of a soft material, such as polydimethylsiloxane (PDMS), using such a mask (Xia & Whitesides 1998). In both cases, patterns are created involving relatively slender beams, which are susceptible to sticking together when a liquid meniscus is introduced since the surface tension of the liquid pulls neighbouring beams together. This can occur when either an etching agent (Mastrangelo & Hsu 1993*a*,*b*; Raccurt *et al.* 2004) or a rinsing agent (Tanaka, Morigami & Atoda 1993; Delamarche *et al.* 1997; Lee *et al.* 2002) dries; the effect is similar in either case. It has also been shown that the 'stiction' caused in this way can sometimes be reversed by rinsing with a different liquid (Delamarche *et al.* 1997).

In this paper we consider the two-dimensional problem of two beams that are clamped to a rigid substrate forming a 'micro-channel' of width w. A finite volume of liquid is deposited at the base of the channel in such a way that the surface of the liquid lies within the channel. The two beams are thus elastically deformed by the surface tension of the interface, as shown schematically in figure 1. In practical applications, deformation can occur because of capillary condensation as well as the rinsing and drying of components (van Spengen, Puers & de Wolf 2002). This may cause a droplet to be stuck near the tip of the beams, a situation that has been studied previously by Kwon *et al.* (2008). However, in general there is no equilibrium configuration with the droplet midway along the beam. For simplicity, therefore, we shall consider the droplet to be in contact with the rigid base of the micro-channel, as shown in figure 1. As a further simplification, we shall neglect the effect of

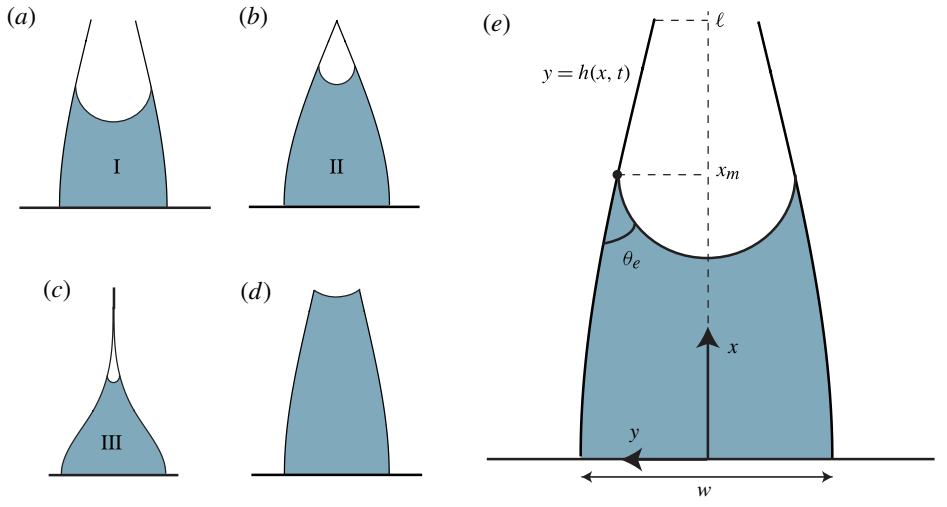

FIGURE 1. (Colour online) (*a–d*) The four possible configurations for a volume of liquid confined between two elastic micro-pillars and a rigid base: (*a*) separated ends, (*b*) touching ends, (*c*) sticking ends, (*d*) fully wetted. This paper considers each of the possibilities in (*a–c*), referred to as regimes I, II and III. (*e*) The notation used in the theoretical formulation of the problem. A two-dimensional micro-channel of width w and length ℓ is filled with a volume v (per unit length) of liquid. The liquid meniscus is located at $x = x_m$ and maintains a constant contact angle θ_e with the beam that makes up the wall of the channel.

evaporation so that the volume of the droplet remains constant. Finally, we neglect the effect of gravity since the micro-channels considered are significantly below the scale at which either hydrostatic pressure within the liquid or the bending of the beams due to their weight become important.

The different configurations that may be adopted by the flexible beams that bound the micro-channel are illustrated in figure 1. We expect that for very small liquid volumes the beams will be bent but remain separated along their length (as depicted in figure 1*a*). As the volume of liquid increases we expect that the distance between the two free ends should decrease. Eventually, we might expect the two beams to touch (see figure 1*b*) or even 'stick' along a finite portion of their length (figure 1*c*). We note that the model we develop does not include an adhesive force between the two beams. However, this geometrical sticking caused by the macroscopic liquid meniscus allows the beams to come into close enough contact for microscopic van der Waals forces to become important and stick the beams irreversibly, even if the liquid is subsequently completely removed. It is thus the initial contact between beams that may lead to problems in the operation of MEMS devices. At the largest droplet volumes we expect the beams to be fully wetted by the liquid (figure 1*d*). In this case the concept of an equilibrium contact angle θ_e is not well defined (Mansfield, Sepangi & Eastwood 1997). In principle, the angle that the meniscus makes to the horizontal could be found as part of the solution, but given that, within the context of our model, there is no mechanism (e.g. gravity) to determine the limits of this configuration, we do not consider this regime here.

In this paper, we investigate the conditions under which each of the three configurations in figure 1(*a–c*) are observed. We show that in certain circumstances

several different equilibrium configurations exist; to investigate which of these is realized we develop a model of the liquid flow based on lubrication theory. We then perform a stability analysis, which demonstrates that multiple stable equilibria may exist. Using full numerical solutions of the dynamic problem, we show that which equilibrium the system reaches then depends on the initial condition for the system. While the existence of multiple equilibria has been reported in related systems previously (see Mastrangelo & Hsu 1993*a*; Py *et al.* 2007; Kwon *et al.* 2008, for example) ours is, to the best of our knowledge, the first study that makes use of a dynamic model to investigate the stability of these multiple equilibria. In particular, this demonstrates that the system does not necessarily tend to the global minimum of energy.

The plan of the paper is as follows. In § 2 we describe our theoretical formulation of the problem by developing a lubrication model for the motion of liquid trapped within a micro-channel, and obtain the equations governing the equilibrium situation as the steady limit of the dynamic problem. We then consider two different values for the equilibrium contact angle θ_e, allowing us to isolate two different force contributions arising from surface tension. In § 3 we study the case $\theta_e = 0$, where surface tension causes a capillary pressure to act along the wetted length of the beam but no line force. In § 4 we briefly consider the case $\theta_e = \pi/2$, where surface tension causes a line force to act at the contact line, modifying some of the scaling results. Finally, in § 5 we summarize our results and consider briefly their practical implications.

2. Theoretical formulation

2.1. *Beams subject to surface tension forces*

We consider the two-dimensional situation shown in figure 1(*e*): a volume per unit length v of liquid is placed between two elastic beams of length ℓ clamped a distance w apart. We imagine that the contact line is at a position x_m and that the contact angle of the liquid has an equilibrium value θ_e, which we shall assume to be the same as that on a rigid solid (see appendix A). We assume that the gradient of the beam deflections remain small throughout so that we may use linear beam theory (see, for example, Landau & Lifschitz 1959) to describe the shape of each beam. Two forces act on each beam as a result of the surface tension γ of the liquid: a line force $\gamma \sin\theta_e$ acts at the contact line, and a capillary pressure force $\gamma\kappa$ due to the curvature κ of the interface, acts just beneath the contact line. In equilibrium, the pressure within the liquid is uniform and so this capillary pressure acts all along the wetted length of the beam. We note that the majority of previous analyses have neglected the line force and focused instead on the force arising from the integrated curvature pressure, although Farshid Chini & Amirfazli (2010) considered both.

For deformations of the beams with small slope, the beam equation (Landau & Lifschitz 1959) governs the shape of each beam $y = h(x)$ incorporating both bending stiffness and tension according to

$$Bh''''(x) + \tau(x)h''(x) = p(x) - \gamma \sin\theta_e \delta(x - x_m). \tag{2.1}$$

Here $B = Eb^3/12(1-\nu^2)$ is the bending stiffness per unit length of the beam, which has thickness b, Young's modulus E and Poisson ratio ν, and the loading pressure is given by

$$p(x) = \begin{cases} p_{liquid}, & 0 < x < x_m, \\ 0, & x_m < x < \ell, \end{cases} \tag{2.2}$$

with p_{liquid} the pressure within the liquid (measured relative to the atmospheric pressure). The Dirac delta function, $\delta(x)$, accounts for the line force arising from surface tension γ. Surface tension, together with the inextensibility of the beam, generates a tension along the beam

$$\tau(x) = \begin{cases} \gamma\cos\theta_e, & 0 < x < x_m, \\ 0, & x_m < x < \ell. \end{cases} \tag{2.3}$$

While we retain this tension for the time being, we shall see in § 2.3 that it may be neglected.

We note that in deriving (2.1) we have neglected the weight of the beam, which is justified provided that the length of the beam is not long enough for it to buckle under its own weight; this requires that $\mathscr{G} = \rho_s g b \ell^3/B \ll 1$, with ρ_s the solid density. We also neglect the hydrostatic pressure within the liquid; this again amounts to neglecting gravity, an assumption that requires the Bond number $Bo = \rho g w^2/\gamma \ll 1$, with ρ the liquid density. (Typically, we envisage that $\rho \sim \rho_s \sim 10^3$ kg m^{-3}, $b \sim w \sim 10$ μm, $\ell \sim 100$ μm, $E > 1$ MPa and $\gamma \sim 10^{-1}$ N m^{-1}, so that $\mathscr{G} \lesssim 10^{-3} \ll 1$ and $Bo \sim 10^{-5} \ll 1$.) For static configurations, therefore, the pressure within the liquid, p_{liquid}, is uniform and is determined by the radius of curvature of the meniscus. Using elementary geometry and the assumption that the slope of the beam is small (which has already been made above) we find that the radius of curvature of this circular arc is $R = h(x_m)/[\cos\theta_e - h_x(x_m)\sin\theta_e]$, and so the pressure within the liquid is

$$p_{liquid} = -\frac{\gamma}{h(x_m)}[\cos\theta_e - h_x(x_m)\sin\theta_e]. \tag{2.4}$$

We note that (2.1) may be derived formally from a variational principle in which the sum of the elastic and surface energies of the system is minimized subject to the constraint of fixed liquid volume; some of the details of this calculation in the simplified case $\theta_e = 0$ are given in appendix A.

2.2. *A dynamic model*

The static model given in § 2.1 will allow us to understand the different equilibrium configurations of beams. However, more generally we are interested in investigating the motion of the beams in non-equilibrium situations and so require a model that couples the motion of the beams to the motion of the liquid within the channel. We neglect the inertia of the beams because of the microscopic scale of most practical applications; this may be formally justified provided $\rho_s/E \ll (t_s/\ell)^2$, where t_s is the viscous time scale of the fluid flow. Similarly, and because of the small width-to-length ratio of many channels used in practice, we develop a dynamic model based on lubrication theory within the thin channel gap. Following the standard approximation of the equations of motion in this limit (see Leal 2007, for example), the pressure p and liquid velocity (u, v) satisfy

$$\frac{\partial p}{\partial x} = \mu\frac{\partial^2 u}{\partial y^2}, \quad \frac{\partial p}{\partial y} = 0, \quad \frac{\partial u}{\partial x} + \frac{\partial v}{\partial y} = 0. \tag{2.5a,b,c}$$

Using no-slip boundary conditions at $y = \pm h$, we may solve (2.5*a*,*b*) for the velocity $u(x, y, t)$, which may then be integrated from $y = 0$ to $y = h(x, t)$ to obtain the half-flux

$$Q = -\frac{h^3}{3\mu}\frac{\partial p}{\partial x}. \tag{2.6}$$

Since the inertia of the beam is negligible, the pressure $p(x,t)$ is given by the rearranged version of (2.1). Finally, conservation of mass gives an evolution equation for the shape of the beam, $h(x,t)$,

$$\frac{\partial h}{\partial t} = \frac{B}{3\mu}\frac{\partial}{\partial x}\left[h^3\left(\frac{\partial^5 h}{\partial x^5} + \frac{\tau}{B}\frac{\partial^3 h}{\partial x^3}\right)\right], \tag{2.7}$$

valid for $0 < x < x_m$.

Equation (2.7) is to be solved subject to clamped boundary conditions at $x = 0$, i.e.

$$h(0,t) = \frac{w}{2}, \quad \left.\frac{\partial h}{\partial x}\right|_{x=0} = 0 \tag{2.8}$$

as well as the requirement that there be no liquid flux through the rigid boundary at $x = 0$, which, using (2.6) with (2.1), gives

$$\left(\frac{\partial^5 h}{\partial x^5} + \frac{\tau}{B}\frac{\partial^3 h}{\partial x^3}\right)_{x=0} = 0. \tag{2.9}$$

At the meniscus $x = x_m$ the pressure within the liquid is given by the curvature of the meniscus, and so we have

$$\left(\frac{\partial^4 h}{\partial x^4} + \frac{\tau}{B}\frac{\partial^2 h}{\partial x^2}\right)_{x=x_m} = -\frac{\gamma}{Bh(x_m)}\left[\cos\theta_e - h_x(x_m)\sin\theta_e\right]. \tag{2.10}$$

Continuity for the shape between the wet and dry portions of the beam requires

$$[h]_-^+ = \left[\frac{\partial h}{\partial x}\right]_-^+ = \left[\frac{\partial^2 h}{\partial x^2}\right]_-^+ = 0, \quad \left[\frac{\partial^3 h}{\partial x^3}\right]_-^+ = -\frac{\gamma\sin\theta_e}{B}, \tag{2.11}$$

where $[f]_-^+ \equiv f(x_m^+,t) - f(x_m^-,t)$.

The shape of the dry portion of the beam satisfies

$$B\frac{\partial^4 h}{\partial x^4} + \tau\frac{\partial^2 h}{\partial x^2} = 0, \tag{2.12}$$

with boundary conditions at the end of the beam, $x = \ell$, depending on which of the configurations shown in figure 1 the beams adopt. When the ends are separated, they are 'free' with zero bending moment and shear (Landau & Lifschitz 1959), so that

$$\frac{\partial^2 h}{\partial x^2} = \frac{\partial^3 h}{\partial x^3} = 0, \quad x = \ell. \tag{2.13}$$

However, for some parameter values we expect that the ends of the beams will touch, in which case 'hinged' boundary conditions are appropriate, i.e.

$$h(\ell,t) = \left.\frac{\partial^2 h}{\partial x^2}\right|_{x=\ell} = 0. \tag{2.14}$$

For still other parameter values we expect that the ends might stick along some portion of their length $x_c < x < \ell$ (see figure 1*c*), and so

$$h(x_c,t) = \left.\frac{\partial h}{\partial x}\right|_{x=x_c} = \left.\frac{\partial^2 h}{\partial x^2}\right|_{x=x_c} = 0 \tag{2.15}$$

for some x_c satisfying $x_m < x_c < \ell$. Note that the continuity of $\partial^2 h/\partial x^2$ at $x = x_c$ ensures that there is no adhesive force between the two beams (Majidi 2007).

The problem is then fully specified apart from the position of the contact line x_m. This may be found either from the local conservation of mass at the contact line or by the requirement that the total volume of liquid, given by

$$\frac{v}{2} = \int_0^{x_m} h \, \mathrm{d}x - h\,(x_m)^2\, v_m(h_x(x_m), \theta_e), \tag{2.16}$$

is conserved. We note that the second term in (2.16) denotes the volume of liquid that is displaced by the meniscus, with v_m a dimensionless, geometric function that may be calculated using elementary geometry. Setting $\mathrm{d}v/\mathrm{d}t = 0$, we find that

$$h(x_m, t)\frac{\mathrm{d}x_m}{\mathrm{d}t} = \frac{\mathrm{d}}{\mathrm{d}t}[h\,(x_m)^2\, v_m] - \frac{B}{\mu}\frac{h\,(x_m, t)^3}{3}\left(\frac{\partial^5 h}{\partial x^5} + \frac{\tau}{B}\frac{\partial^3 h}{\partial x^3}\right)\Bigg|_{x_m}. \tag{2.17}$$

In situations where the volume displaced by the meniscus may be neglected, this condition simply states that the speed of the contact line matches the depth-averaged velocity there. We note that we may ignore the details of the moving contact line, at which there is necessarily a stress singularity that must be regularized, provided the capillary number is small (see § 2.3 for more justification). In this limit the leading-order problem away from the contact line depends only on the macroscopic contact angle (Weinstein, Dussan & Ungar 1990). We emphasize that in this paper we assume for simplicity that the contact angle retains its equilibrium value θ_e and is not related to the speed at which the contact line moves. Finally, we note that for some parameter values we might expect that the meniscus reaches the end of the beam. As noted in § 1, we do not allow this possibility here and so terminate the simulations if the meniscus reaches the end of the beam.

2.3. *Scaling analysis*

We now determine, in scaling terms, the beam length for which we expect surface tension to cause the two beams to interact. We note that the second term on the right-hand side of (2.4) may be neglected provided θ_e is not close to $\pi/2$. Taking the limiting case of $\theta_e = 0$, for which there is a pure curvature pressure (no line force), we may find a scaling relationship for the critical beam length ℓ_c at which interactions between the two beams (i.e. touching and sticking) should occur by balancing (2.1) to yield $Bw/\ell_c^4 \sim \gamma/w$, and so

$$\ell_{c,0} \sim w^{1/2}\ell_{ec}^{1/2}, \tag{2.18}$$

where $\ell_{ec} = (B/\gamma)^{1/2}$ is the *elastocapillary length* (Bico *et al.* 2004) and measures the competition between bending and surface energies.

At the other end of the spectrum, we may take $\theta_e = \pi/2$. Integrating (2.1) once (to eliminate the δ-function) the analogous scaling becomes $Bw/\ell_c^3 \sim \gamma$, so that

$$\ell_{c,\pi/2} \sim w^{1/3}\ell_{ec}^{2/3}. \tag{2.19}$$

We note that the scaling laws in (2.18) and (2.19), whilst being qualitatively similar, are quantitatively different; while the scaling law (2.18) for $\theta_e = 0$ has frequently been given in the literature (see, for example, Bico *et al.* 2004), we are unaware of other occurrences of the scaling (2.19) for $\theta_e = \pi/2$ having been given. However, we note that our use of beam theory requires that $w/\ell_c \ll 1$ so that $w \ll \ell_{ec}$ and hence $\ell_{c,0} \ll \ell_{c,\pi/2}$. We thus expect that for intermediate values of θ_e it should be the scaling (2.18) that is the most pertinent.

Furthermore, we note that, when the length of the beams is such that surface tension causes them to interact, the ratio of the tension to bending stiffness terms in (2.1) scales like $(\tau w/\ell_c^2)/(Bw/\ell_c^4) \sim \ell_c^2/\ell_{ec}^2$. Using the scaling (2.18) to eliminate ℓ_{ec}, we have that this ratio scales like w^2/ℓ_c^2. Given that our use of both beam theory and lubrication theory in deriving the governing equations requires that the slope of the beam at the critical length for touching $w/\ell_c \ll 1$, it is therefore entirely consistent to neglect the beam tension. We set $\tau = 0$ henceforth. (We note that we are therefore neglecting the possibility that the beam will buckle because of surface tension, and considering only bending. A scenario in which each of these possibilities is realized by changing the contact angle is studied by Andreotti *et al.* 2011). In the same way, the ratio of the volume displaced by the meniscus to the total volume of liquid scales like w/ℓ, and so may also be neglected in (2.17). Finally, choosing the time scale t_s such that the first two terms in (2.7) balance, we see that the capillary number $Ca \sim \mu\ell/\gamma t_s \sim w/\ell_c \ll 1$. The rate of viscous dissipation near the contact line is given, up to a logarithmic factor, by $\mathscr{D}_{cl} \sim \gamma^2 Ca^{5/3}/\mu$ (see de Gennes, Brochard-Wyart & Quéré 2003, for example). Meanwhile the rate of viscous dissipation within the bulk is $\mathscr{D}_b \sim \mu \int_V (\partial u/\partial y)^2 \, \mathrm{d}V \sim w^3 \ell \, (\partial p/\partial x)^2 / \mu \sim B^2 w^5/\mu\ell^9$. Thus, $\mathscr{D}_{cl}/\mathscr{D}_b \sim (w/\ell)^{2/3} \ll 1$ and viscous dissipation at the contact line is negligible in comparison with that in the bulk; this justifies our neglect of a dynamic contact angle.

2.4. *Non-dimensionalization*

With the above simplifications, we now non-dimensionalize all space variables with the elastocapillary length $\ell_{ec} = (B/\gamma)^{1/2}$ and time with the elastocapillary time $t_{ec} \equiv \mu\ell_{ec}/\gamma$. In particular, we let

$$H(X,T) = h(x,t)/\ell_{ec}, \quad (L,W,X) = (\ell,w,x)/\ell_{ec}, \quad T = t/t_{ec}, \quad P = p\ell_{ec}/\gamma. \tag{2.20}$$

With this choice of dimensionless variables, (2.7) becomes

$$\frac{\partial H}{\partial T} = \frac{1}{3}\frac{\partial}{\partial X}\left(H^3 \frac{\partial^5 H}{\partial X^5}\right), \tag{2.21}$$

subject to the boundary conditions

$$H(0,T) = \frac{W}{2}, \quad H_X(0,T) = H_{XXXXX}(0,T) = 0, \tag{2.22a,b,c}$$

and

$$[H]_-^+ = [H_X]_-^+ = [H_{XX}]_-^+ = 0, \quad [H_{XXX}]_-^+ = -\sin\theta_e, \quad H_{XXXX}(X_m,T) = -\frac{\cos\theta_e}{H(X_m)}, \tag{2.23}$$

where $[F]_-^+ \equiv F(X_m^+,T) - F(X_m^-,T)$, as well as the appropriate conditions at the dry end of the beam, namely

$$H_{XX}(L,T) = H_{XXX}(L,T) = 0 \quad \text{(separated ends)}, \tag{2.24a}$$

$$H(L,T) = H_{XX}(L,T) = 0 \quad \text{(touching ends)}, \tag{2.24b}$$

$$H(X_c,T) = H_X(X_c,T) = H_{XX}(X_c,T) = 0 \quad \text{(sticking ends)}. \tag{2.24c}$$

The position of the contact line $X_m(T)$ evolves according to the dimensionless version of (2.17), which reads

$$\frac{\mathrm{d}X_m}{\mathrm{d}T} = -\frac{H(X_m,T)^2}{3}\frac{\partial^5 H}{\partial X^5}\bigg|_{X_m}. \tag{2.25}$$

Finally, we must specify an initial condition $H(X,0) = H_0(X)$ and find an initial meniscus position $X_m(0)$ that satisfies the constraint on the volume of liquid trapped between the beams, i.e.

$$\frac{V}{2} = \int_0^{X_m(0)} H_0(X)\,\mathrm{d}X. \tag{2.26}$$

We note that our governing equation and boundary conditions are equivalent to those studied in Aristoff *et al.* (2011) except for boundary condition (2.22*c*), which ensures that the amount of fluid between the two beams remains constant. Aristoff *et al.* (2011) were studying a problem in which the end $x = 0$ is open to a bath of liquid so that a zero pressure condition at the clamped end $x = 0$ was appropriate, rather than our no-flux condition (2.22*c*).

The evolution equation (2.21) is to be solved on the evolving interval $0 \leqslant X \leqslant X_m(T)$. To facilitate the numerical solution of this equation we let $Z = X/X_m(T) \in [0,1]$ (this is modified to $Z = X/X_c(T)$ when the ends of the beams stick, as in figure 1*c*), transforming (2.21) to

$$\frac{\partial H}{\partial T} = \frac{\dot{X}_m Z}{X_m}\frac{\partial H}{\partial Z} + \frac{1}{3X_m^6}\frac{\partial}{\partial Z}\left[H^3\left(\frac{\partial^5 H}{\partial Z^5}\right)\right], \tag{2.27}$$

where $\dot{()}$ denotes $\mathrm{d}()/\mathrm{d}T$. Note that the transformation to the rescaled interval $0 \leqslant Z \leqslant 1$ introduces an additional advective term in (2.27) that does not appear in the presentation of Aristoff *et al.* (2011). Equation (2.27) is then solved on a fixed mesh using the method of lines; further details of the numerical scheme employed may be found in appendix B. The volume of liquid is monitored to give an indication of the numerical errors introduced; it is found to remain within 0.01 % of its initial value for all simulations reported here.

2.5. *Equations for equilibrium*

The special case of equilibrium may be recovered from the steady case of the dynamic problem given by (2.21) or by returning to the original beam equation. We have that the equilibrium beam shape $Y = H_e(X)$ satisfies

$$\frac{\mathrm{d}^4 H_e}{\mathrm{d}X^4} = P(X) - \sin\theta_e \delta(X - X_m), \tag{2.28}$$

where

$$P(X) = \begin{cases} -\dfrac{1}{H_e(X_m)}[\cos\theta_e - H_e'(X_m)\sin\theta_e], & 0 \leqslant X < X_m, \\ 0, & X_m \leqslant X \leqslant L. \end{cases} \tag{2.29}$$

To determine the equilibrium shape of the beam, we solve (2.28)–(2.29) subject to the boundary conditions (2.22)–(2.23) (with $H(X,T)$ replaced by $H_e(X)$) at $X = 0, X_m$, and the appropriate conditions from (2.24*a–c*) at $X = L$. The volume of liquid for a given equilibrium shape can then be found from (2.26).

3. A pure curvature force: $\theta_e = 0$

In this section we isolate the effect of the curvature force compared to the line force from surface tension by setting $\theta_e = 0$. For the static problem, we shall assume that the position of the meniscus $X_m < L$ is given, calculate the corresponding equilibrium

shape $H_e(X; X_m)$ and then calculate the volume $V(X_m)$ required to produce this meniscus position using (2.26). This approach facilitates the calculation, though in reality we expect that it is the volume of liquid V that is given and hence that the meniscus will move until it is at the equilibrium position for that volume (subject to the constraint that the meniscus location does not reach the end of the beam, i.e. $X_m/L < 1$).

3.1. *Equilibrium configurations*

We begin by considering each of the three different possibilities illustrated in figure 1 in turn before then combining these results into a regime diagram illustrating when each of these possibilities may be realized. However, recalling the scaling law (2.18) leads us to expect that the typical horizontal length scale for $\theta_e = 0$ is $L_c \sim W^{1/2}$. A consequence of this is that the three-dimensional parameter space (W, V, L) can be reduced to a two-dimensional parameter space by letting $\omega = W/L^2$ and $\nu = V/L^3$. We therefore introduce the rescaled variables $\eta = H/L^2$, $\eta_e = H_e/L^2$, $\xi = X/L$, $\xi_m = X_m/L$ and make use of this rescaling in what follows.

3.1.1. *Regime I: separated ends*

By solving (2.28)–(2.29) with boundary conditions (2.24*a*) we find that the rescaled equilibrium beam shape $\eta_e = H_e/L^2$ is given by

$$\eta_e(\xi; \xi_m) = \begin{cases} \eta_m + \dfrac{1}{24\eta_m}[4\xi_m^3(\xi_m - \xi) - (\xi_m - \xi)^4], & 0 < \xi < \xi_m, \\ \eta_m + \dfrac{\xi_m^3}{6\eta_m}(\xi_m - \xi), & \xi_m < \xi < 1, \end{cases} \tag{3.1}$$

with the deformation at the meniscus, η_m, satisfying

$$\eta_m^2 - \frac{\omega}{2}\eta_m + \frac{\xi_m^4}{8} = 0. \tag{3.2}$$

For this solution to be valid we require that the beam ends do not touch, i.e. that $\eta_e(1) > 0$, and hence $\xi_m = X_m/L$ must satisfy

$$\omega\eta_m > \frac{\xi_m^3}{12}(4 - \xi_m). \tag{3.3}$$

Finally, the (rescaled) volume is given by

$$\nu = 2\eta_m\xi_m + \frac{3}{20}\frac{\xi_m^5}{\eta_m}, \tag{3.4}$$

where we have neglected the volume of liquid that is displaced by the meniscus, as discussed in § 2.3.

3.1.2. *Regime II: touching ends*

By solving (2.28)–(2.29) with boundary conditions (2.24*b*) we find that the beam shape is given by

$$\eta_e(\xi; \xi_m) = \begin{cases} -\dfrac{(\xi_m - \xi)^4}{24\eta_m} + A(1 - \xi) + B(1 - \xi)^3, & 0 < \xi < \xi_m, \\ A(1 - \xi) + B(1 - \xi)^3, & \xi_m < \xi < 1, \end{cases} \tag{3.5}$$

where

$$A = \frac{3\omega}{4} + \frac{\xi_m^3}{48\eta_m}(3\xi_m - 4), \quad B = \frac{1}{3}\left(\frac{\xi_m^3}{6\eta_m} - A\right), \tag{3.6}$$

and the rescaled meniscus radius η_m is the solution of the quadratic equation

$$\eta_m^2 - \frac{\omega}{2}(1-\xi_m)(1+\xi_m - \xi_m^2/2)\eta_m + \frac{\xi_m^4}{48}(1-\xi_m)(6-6\xi_m+\xi_m^2) = 0. \tag{3.7}$$

The corresponding volume of liquid trapped is given by

$$v = -\frac{\xi_m^5}{60\eta_m} + A\xi_m(2-\xi_m) + \frac{1}{2}B\xi_m(4-6\xi_m+4\xi_m^2-\xi_m^3). \tag{3.8}$$

To have physical solutions in this regime, we must have that the slope of the beam at the end be negative, i.e. $A > 0$. Furthermore, we must also ensure that the reaction force is in the negative sense (i.e. is a repulsive, rather than attractive, force). Hence we also require that $B > 0$. To satisfy both of these constraints, we require that

$$\frac{1}{12}\left(\frac{4}{3} - \xi_m\right)\xi_m^3 < \omega\eta_m < \frac{1}{12}(4-\xi_m)\,\xi_m^3. \tag{3.9}$$

3.1.3. *Regime III: sticking ends*

In the event that the ends of the beams 'stick', the first contact occurs at some unknown position $\xi = \xi_c = X_c/L$. Solving (2.28)–(2.29) with boundary conditions (2.24*c*) we find that the beam shape is given by

$$\eta_e(\xi;\xi_m) = \begin{cases} -\dfrac{1}{24\eta_m}(\xi_m-\xi)^4 + A(\xi_c-\xi)^3, & 0 < \xi < \xi_m, \\ A(\xi_c-\xi)^3, & \xi_m < \xi < \xi_c, \end{cases} \tag{3.10}$$

where

$$A\xi_c^3 = \frac{\omega}{2} + \frac{\xi_m^4}{24\eta_m}, \quad \xi_c = \frac{3}{4}\xi_m + 9\frac{\omega\eta_m}{\xi_m^3}, \tag{3.11}$$

with ξ_c and η_m being found as the solution of the quartic

$$18\eta_m^2 = \frac{(9\omega\eta_m - \xi_m^4/4)^3}{(3\xi_m^4/4 + 9\omega\eta_m)^2}. \tag{3.12}$$

The corresponding liquid volume is given by

$$v = -\frac{\xi_m^5}{60\eta_m} + \frac{1}{4}\left(\omega + \frac{\xi_m^4}{12\eta_m}\right)\xi_c\left[1 - \left(\frac{\xi_c - \xi_m}{\xi_c}\right)^4\right]. \tag{3.13}$$

For this solution to be physically realistic we need to ensure that $\xi_m < \xi_c < 1$, which using (3.11) may easily be rearranged to give

$$\tfrac{1}{36}\xi_m^4 < \omega\eta_m < \tfrac{1}{12}\xi_m^3(\tfrac{4}{3} - \xi_m). \tag{3.14}$$

We note that the reaction force in this configuration is always repulsive (as desired) since $A > 0$ in (3.11).

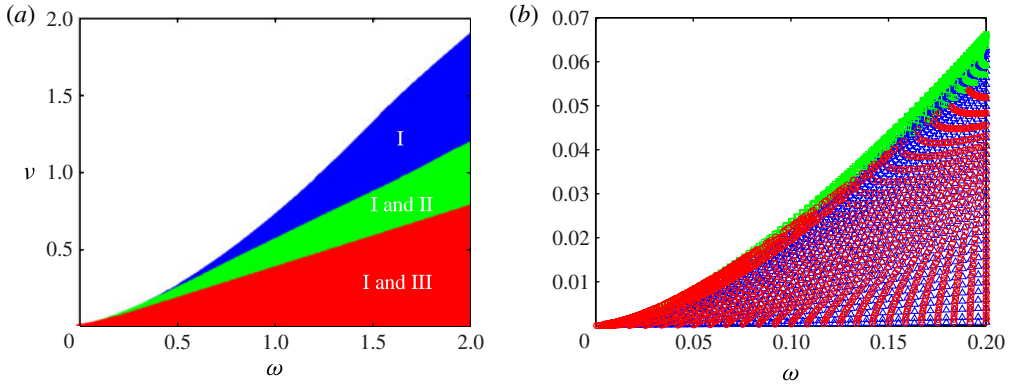

FIGURE 2. (Colour online) (*a*) Regime diagram showing the regions of (ω, ν) parameter space for which each of the various equilibrium beam configurations are observed for $\theta_e = 0$. (*b*) A close-up of the bottom left of (*a*) showing that there are regions in which only regimes II or III are possible. Points corresponding to regimes I, II, and II are plotted as triangles, squares, and circles, respectively.

3.1.4. *Regime diagram*

Here we collate the restrictions on ν and ω derived above to present a regime diagram describing when each of the three regimes I, II and III are observed. Now, the inequalities (3.3), (3.9) and (3.14) involve not just ω and ν but also η_m, which itself is a function of both ω and ξ_m. We are therefore unable to construct simple inequalities to characterize the (ω, ν) parameter space and so explore the possible existence of equilibrium states by numerical means. We show in figure 2 the regime diagram computed numerically using $O(10^4)$ points. We note that there appear to be regions of (ω, ν) parameter space for which multiple regimes are possible. Indeed, provided an equilibrium exists, there appear to always be two possible configurations, possibly of the same type, while there is a small region for which four solutions exist (two in regime I and two in regime II). We shall discuss subsequently which of the different equilibrium states the system in fact chooses.

Some examples of the multiplicity of equilibrium states are shown in figure 3. In this case $\omega = 0.02$, and we see that by increasing the volume of liquid we pass from the coexistence of a regime I and a regime III equilibrium state, to the coexistence of a regime II and a regime III state, to two regime III states. Finally, there is too much liquid and no equilibrium states exist.

3.2. *Dynamic results*

To understand the stability of the multiple equilibria shown in figure 3, as well as which equilibrium state results from a given initial condition, we use the dynamic model developed in § 2.4. Typically, we take $\eta_0(\xi) = \omega/2$ and $\xi_m(0) = \nu/\omega$ as the initial condition in our numerical scheme (described in more detail in appendix B). The boundary conditions at the ends of the beam are those appropriate to the last known configuration of the beam, and the transition between configurations, e.g. from separated ends to touching ends, is captured using event location within MATLAB. A simple example of the evolution of a system that undergoes this transition is shown in figure 4(*a*), where we have chosen $\omega = 0.02$, $\nu = 0.0021$ as in figure 3(*c*). In this case, the beam shape evolves and the contact line moves monotonically towards the final sticking equilibrium predicted by the regime diagram; the evolution of $\xi_m(T)$ is shown

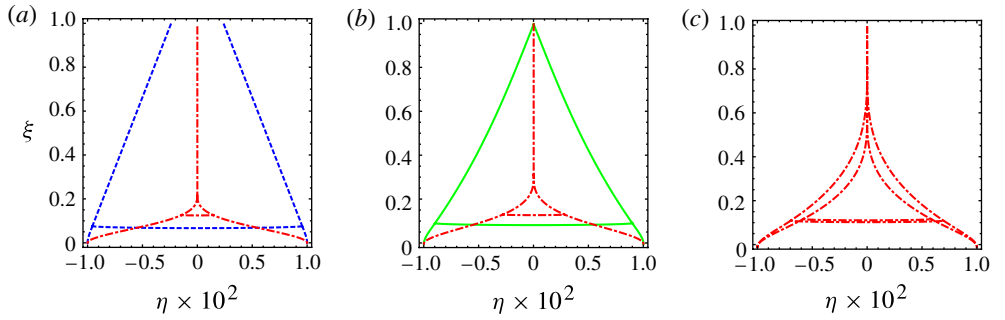

FIGURE 3. (Colour online) Three examples of the multiple equilibria that exist with $\theta_e = 0$ and $\omega = 0.02$. In (*a*) $\nu = 0.0015$: an equilibrium in regime I ($\xi_m \approx 0.076$) coexists with one in regime III ($\xi_m \approx 0.126$). In (*b*) $\nu = 0.0018$ and an equilibrium in regime II ($\xi_m = 0.0939$) coexists with one in regime III ($\xi_m \approx 0.133$). In (*c*) $\nu = 0.0021$ and two equilibria in regime III coexist ($\xi_m \approx 0.120, 0.127$). In each plot the three regimes are differentiated using different line styles as follows: regime I (dashed), regime II (solid), and regime III (dot-dashed). Note that the shapes of both the menisci and the bent beams are shown. The menisci are, in fact, semicircular but appear almost horizontal because of the difference in horizontal and vertical scales.

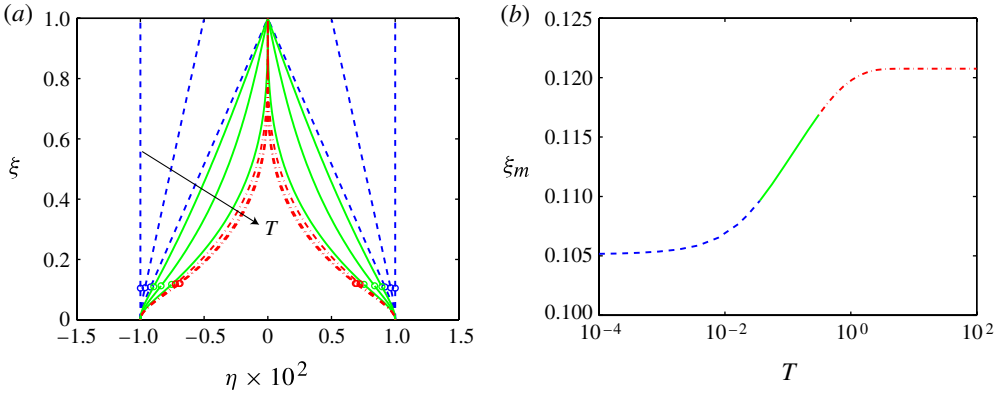

FIGURE 4. (Colour online) Evolution towards equilibrium starting from initially straight beams $\eta_0(\xi) = \omega/2$, taking $\omega = 0.02$, $\nu = 0.0021$. In (*a*) we show the beam evolution towards its steady-state equilibrium with sticking ends (regime III). The direction of increasing time is shown by the arrow, while the position of the meniscus $\xi = \xi_m$ is indicated by circles, with a plot of $\xi_m(T)$ shown in (*b*) using a logarithmic time scale. In each plot the configuration regime is indicated by the use of different line styles, as follows: regime I (dashed), regime II (solid) and regime III (dot-dashed).

in figure 4(*b*). We note that if the volume is increased too much ($\nu_{\max} \approx 0.00211$ for $\omega = 0.02$) the beams go through the same pattern of changes to their configuration before the meniscus finally reaches the end of the beam, at which point our simulation stops, as discussed in § 2.2.

For cases in which there are exactly two equilibrium states, the system is observed to always evolve to the same equilibrium state – the other equilibrium is unstable. For a more interesting example we take $\omega = 0.6$, $\nu = 0.3$, for which four different

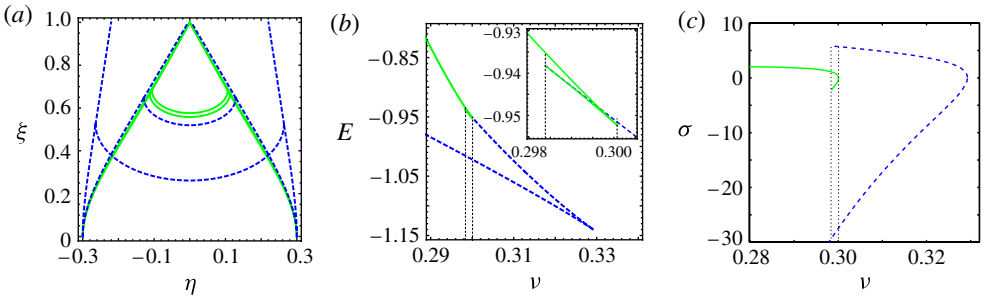

FIGURE 5. (Colour online) Results for $\theta_e = 0$ and $\omega = 0.6$. (*a*) An equilibrium scenario in which four steady states are possible with $\nu = 0.3$. (*b*) Total energy of the equilibria and (*c*) growth rate σ of perturbations to the equilibrium solutions as functions of ν. In all cases, the curves corresponding to regime I steady states are dashed, while those corresponding to regime II steady states are solid. The dotted lines in (*b,c*) indicate the range of volumes for which four equilibrium states are possible.

equilibrium states are possible, as plotted in figure 5(*a*). We first investigate the stability of each of these equilibria numerically by adding a small sinusoidal perturbation to the equilibrium shape and setting this as the initial condition. We find that two of these equilibria, one in regime I (separated ends) and one in regime II (touching ends) are stable, but the other two are unstable: the perturbed unstable regime I solution evolves to one of the two stable equilibria, while the perturbed unstable regime II solution evolves either to the stable regime II state or $\xi \to 1$ and the simulation stops. Which of these situations occurs depends on the sign of the beam's slope at ξ_m. An example of the evolution away from an unstable equilibrium towards one of the two stable equilibria is shown in figure 6(*a*).

3.3. *Energy of the system*

It is interesting to compare this behaviour with what might have been expected on the basis of the total energy of the system. In this case, $\theta_e = 0$, the total energy (bending plus surface energy) may be written

$$E = \int_0^1 \frac{1}{2}\eta_{\xi\xi}^2 \,\mathrm{d}\xi - \xi_m. \tag{3.15}$$

Here the first term represents the bending energy of the beam and the second term arises because of the difference in solid–liquid and solid–vapour surface energies. However, the surface energy of the meniscus itself must be neglected for consistency with the small-slope approximation used throughout. We note that this energy applies equally to regime III as to regimes I and II since our model does not account for an additional attractive or repulsive force between the two beams, which would require a discontinuity in curvature at $\xi = \xi_c$ (Majidi 2007). The energy of the system is plotted as a function of ν in figure 5(*b*) for $\omega = 0.6$. We see that the two equilibrium states with lowest energy are stable, although their energies are not the same. This finding is consistent with the evolution of the total energy of the system; following Jensen (1997), we note that by differentiating (3.15) with respect to time, integrating by parts

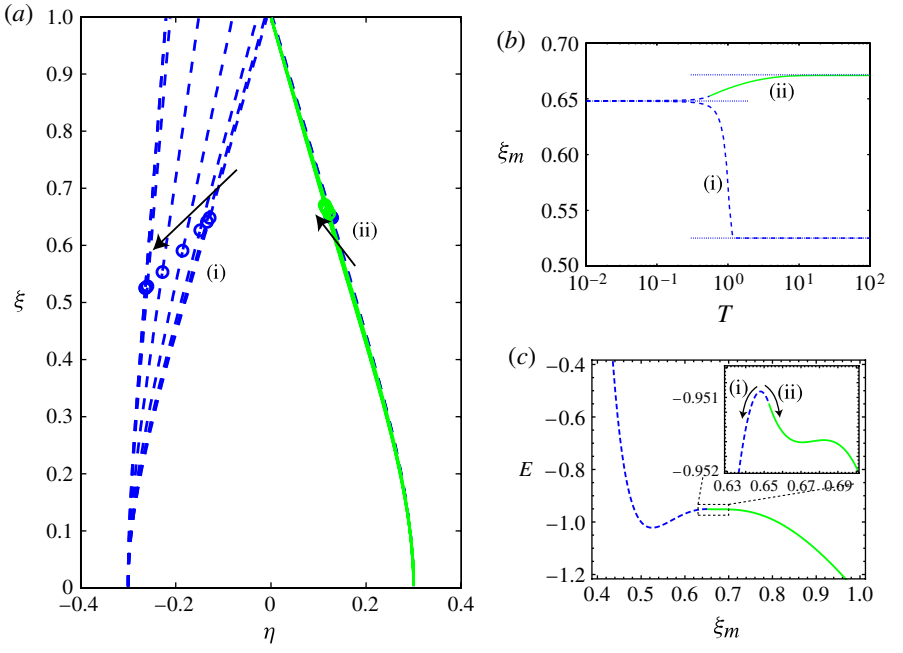

FIGURE 6. (Colour online) (*a*) Dependence on initial conditions in a scenario with multiple equilibria. Here $\nu = 0.3$, $\omega = 0.6$ so that two equilibria in regime II (touching ends) coexist with two equilibria in regime I (see figure 5*a* for the shapes of these equilibria). Only two of these four equilibria are stable: starting with different small perturbations to the unstable regime I equilibrium, the beam shape tends to either (i) the second regime I configuration or (ii) the stable regime II configuration. Arrows show the direction of increasing time T. (*b*) The corresponding behaviours of the meniscus position $\xi_m(T)$ in each case. (*c*) Total energy E as a function of ξ as calculated using the Ritz method (with the inset showing a magnified version of the behaviour for $0.63 \leqslant \xi_m \leqslant 0.7$). In all cases the curves corresponding to regime I (separated ends) are dashed, those corresponding to regime II (touching ends) are solid.

twice, and applying the boundary conditions, the rate of change of energy

$$\frac{\mathrm{d}E}{\mathrm{d}T} = -\int_0^{\xi_m} \frac{1}{3}\eta^3 \eta_{\xi\xi\xi\xi\xi}^2 \,\mathrm{d}\xi \leqslant 0. \tag{3.16}$$

Thus the energy decreases as the flow evolves until it reaches an equilibrium solution for which $\mathrm{d}E/\mathrm{d}T = 0$.

To understand this result further, it is useful to follow Mastrangelo & Hsu (1993*a*) and imagine an energy landscape of the system for constant ν and varying ξ_m. To do this, we use the Ritz method, in which the solution is assumed to be a simple test function that satisfies all of the boundary conditions except the pressure taking its equilibrium value. Such an energy landscape is shown for $\omega = 0.6$, $\nu = 0.3$ in figure 6(*c*), and clearly shows the two maxima and two minima, corresponding precisely to the two unstable and two stable equilibria found here. It is then intuitively obvious that a system perturbed from an equilibrium will flow to the nearest local minimum, the exception to this being if the starting ξ_m is greater than that for the regime II equilibrium with highest ξ_m, in which case the meniscus keeps evolving until

it reaches the end of the beam. These predictions are thus in complete agreement with the full numerical solution.

3.4. *Linear stability analysis*

Although energy considerations are able to predict the stability of the different equilibria, they give no information about the the time scale of the evolution to and from different equilibria. In particular, we note from figure 6(*b*) that the evolution away from the unstable regime I is relatively slow whilst that to the stable regime I is fast. To understand this, we consider small perturbations of the beams from their equilibrium deflection $\eta_e(\xi)$ and equilibrium meniscus position $\xi_m^{(0)}$ by letting

$$\eta(\xi, T) = \eta_e(\xi) + \varepsilon \mathrm{e}^{\sigma T} f(\xi), \quad \xi_m(T) = \xi_m^{(0)} + \varepsilon \mathrm{e}^{\sigma T} \xi_m^{(1)}, \tag{3.17}$$

where $\varepsilon \ll 1$. At first order in ε we find that the rescaled perturbation $g(\xi) = f(\xi)/\xi_m^{(1)}$ satisfies

$$\sigma g = \tfrac{1}{3} \left(\eta_e^3 g''''\right)', \tag{3.18}$$

subject to

$$g = g' = g'''' = 0 \quad \text{at } \xi = 0, \tag{3.19a}$$

$$g'' = \eta_e(\xi_m^{(0)}) g''' - 1 = \eta_e \left(\xi_m^{(0)}\right)^2 g'''' - \eta_e'(\xi_m^{(0)}) - g = 0 \quad \text{at } \xi = \xi_m^{(0)}, \tag{3.19b}$$

$$\int_0^{\xi_m^{(0)}} g(\xi)\, \mathrm{d}\xi + \eta_e(\xi_m^{(0)}) = 0, \tag{3.19c}$$

for the case of separated ends, while (3.19*b*) must be modified accordingly for touching or sticking ends. We note that the form of the boundary conditions in (3.19*b*) results from the Taylor expansion of the boundary conditions about the unperturbed meniscus position.

For $\sigma \neq 0$ we may substitute (3.18) into (3.19*c*) to find

$$\sigma = -\tfrac{1}{3} \eta_e^2 g'''' \quad \text{at } \xi = \xi_m^{(0)}. \tag{3.19d}$$

This expression of the conservation of mass is more convenient for numerical implementation that (3.19*c*) and so is used here.

We solve (3.18)–(3.19) using MATLAB's boundary value solver `bvp4c`, which computes the growth rate σ as part of the solution. We show the results for $\omega = 0.6$, $\nu = 0.3$ in figure 5(*c*). The results are in qualitative agreement with the results from the full numerical solution of our dynamic model: for both regime I and II, the equilibrium with lower ξ_m is stable, while the one with higher ξ_m is unstable. Furthermore, figure 6(*b*) shows that the growth rates σ are consistent with the time scales over which the motion occurs: the instability grows on an $O(1)$ time scale, but the regime I stable equilibrium is reached more quickly than its regime II counterpart; this is consistent with the $O(10)$ difference in the values of σ between the two.

A more typical example with just two steady states is given in figure 7(*b*) for $\omega = 0.02$, and should be compared with the corresponding (E, ν) plot. In general, we observe that where different regimes coexist a regime I equilibrium is always stable (the coexisting regime II or III equilibrium is unstable), while if regime II and III coexist then it is the regime II equilibrium that is stable. This observation is important for practical purposes since it suggests that in general the system will choose a stable equilibrium in either regime I or II while the remaining regime III configuration will be unstable. There is only a very narrow window of parameter space for which only

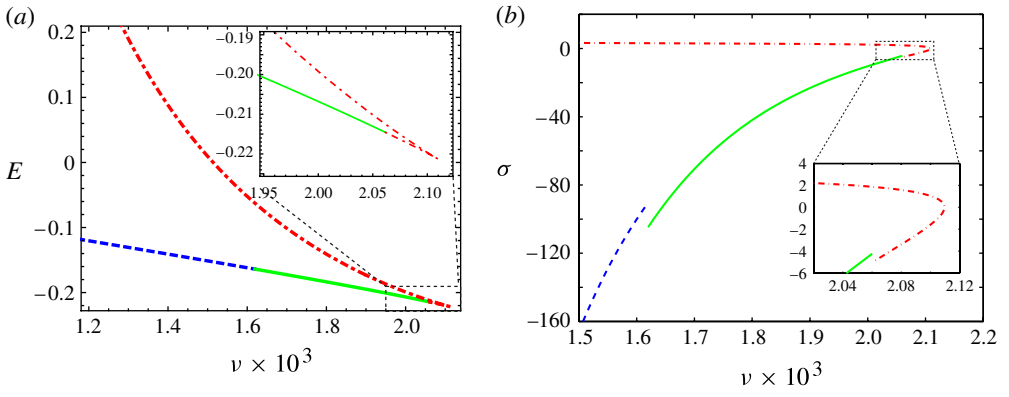

FIGURE 7. (Colour online) (*a*) Total energy of steady states and (*b*) growth rate σ of perturbations to these steady-state shapes as functions of ν for $\omega = 0.02$ and $\theta_e = 0$. Insets show magnification of the region around $\nu = 2 \times 10^{-3}$. In both cases the three regimes are differentiated by using different line styles: regime I (dashed), regime II (solid) and regime III (dot-dashed). Note in (*b*) that the growth rate σ is subject to a discontinuity when the configuration of the beams changes; this is because the boundary conditions at the beam's ends change.

regime III is possible; however, for such parameter values one of the regime III states is stable and the other unstable.

4. The effect of the line force

In this section we consider briefly the effect of the surface-tension-induced line force (compared to the curvature force), and take $\theta_e = \pi/2$; this choice maximizes the importance of the line force. As noted in § 2.3, we find that the critical length ℓ_c at which interactions between the two beams should occur satisfies the new scaling law (2.19). Assuming this scaling law, we now find that the capillary pressure and line force are of the same order, with the beam satisfying

$$h''''(x) = \frac{\gamma}{B}\left[\frac{h_x(x_m)}{h(x_m)} - \delta(x - x_m)\right], \tag{4.1}$$

in $x < x_m$. The presence of the first term on the right-hand side of (4.1) complicates the solution of the beam equation and hence the determination of the inequalities required to present a regime diagram of different equilibrium states. It is therefore of little benefit to do so here, and we note only that all of the analysis and numerical results of § 3 may, in principle, be repeated for $\theta_e = \pi/2$. We expect that in this scenario multiple equilibria will again be observed since the equation for ξ_m as a function of volume of liquid will again be a quartic. More generally, we note that the line force and curvature force terms will balance provided $|\pi/2 - \theta_e| \ll 1$, while for θ_e not close to $\pi/2$ the line force may be neglected and scaling law (2.18) will hold.

5. Discussion

We have presented theoretical results demonstrating how a seemingly simple elastocapillary system (a drop placed between two flexible beams) can exhibit a surprisingly rich behaviour. In particular, we have shown that in certain

circumstances multiple equilibrium configurations exist and that more than one of these configurations can be stable. We have performed a linear stability analysis to predict the stability of these equilibria, and simulations for the full problem to demonstrate that the system evolves to the nearest local energy minimum. This agreement validates the approaches used here as well as the assumptions made on the basis of static models in related situations (Mastrangelo & Hsu 1993*a*).

For simplicity, we restricted ourselves to the case of zero equilibrium contact angle θ_e, so that there is only a pressure force due to the curvature of the interface, with the line force playing no role. It is then relatively simple to characterize the equilibria of the system in terms of just two parameters: the reduced channel width, ω, and the reduced volume of liquid, ν. The regime diagram, presented in figure 2, clearly shows the existence of multiple equilibria, but is more useful once the stability of the equilibria is taken into account. In particular, we see that for sufficiently large ω we expect the system to adopt a configuration with separated ends; although touching/sticking configurations may co-exist with a separated end configuration, they are always unstable. However, such configurations can become stable for ω sufficiently small.

For non-zero values of θ_e the ratio of the line force to the curvature pressure force scales like $\tan\theta_e w/x_m$, and so depends on the contact angle, θ_e, the width of the channel and the volume of liquid deposited. Nevertheless, for thin channels a simple scaling analysis suggests that in most practical situations we expect it to be the curvature pressure that dictates the critical beam length ℓ_c at which touching should occur, giving rise to the well-known scaling law $\ell_c \sim w^{1/2}\ell_{ec}^{1/2}$ (Bico *et al.* 2004). We only expect the line force to contribute to the force balance for contact angles close to $\pi/2$, in which case we predict a new scaling law $\ell_c \sim w^{1/3}\ell_{ec}^{2/3}$. It would be interesting for this prediction to be tested experimentally.

In terms of practical applications in MEMS fabrication, our fixed-volume theory may be relevant to situations involving evaporation provided that the evaporation rate of the rinse liquid is sufficiently slow ($\ll 1/t_{ec}$). In this case, once initial equilibrium is reached, the evolution of the beams as the volume of the drop decreases is quasi-steady. Although our results do not provide an obvious mechanism for the collapse of micro-channels under slow evaporation (i.e. a switch from regime I to regime II or III under decreasing ν), they do show that touching/sticking regimes are to be expected, at least for small ω.

Despite its drawbacks, it is the simple nature of our model that has allowed us to completely characterize the interaction of elastic and capillary forces in this idealized system, and so offers an excellent starting point for theoretical investigations into scenarios with more realistic geometries and physical effects. Other geometries of interest include a whole series of micro-pillars, each one being pulled on either side by its neighbours (Tanaka *et al.* 1993), or a two-dimensional array of micro-pillars, as in the experiments of Chandra & Yang (2009) and Pokroy *et al.* (2009). In the channel geometry studied here, effects in the (neglected) third dimension may play an important role. For example, the analysis of Roy & Schwartz (1999) suggests that a cylindrical channel of liquid will be subject to the Rayleigh–Plateau instability if the capillary pressure decreases as the cross-sectional area of the liquid increases. In the scenario investigated here, this criterion is fulfilled since the ends of the beam come closer together and the radius of curvature of the meniscus increases. However, the ability of the beams to bend along their length might mean that this instability is suppressed. We leave consideration of the effect of more complicated geometries as an open question.

Acknowledgements

This publication was based on work supported in part by Award No KUK-C1-013-04, made by King Abdullah University of Science and Technology (KAUST). We also thank M. Mihelich for his contribution to the early stages of this work as a summer student supported by an Oppenheimer Early Career Fellowship (D.V.), and K. Singh for comments on an earlier draft. Finally, we thank O. E. Jensen for pointing out a discrepancy in earlier versions of our energy calculation.

Appendix A. A variational principle

The total energy of the system consists of the bending energy of the beam and the surface energies of the solid–liquid, solid-vapour, and liquid–vapour interfaces. We thus have

$$E(h) = \int_0^{x_e} \frac{B}{2} h_{xx}^2 \left(1 - \frac{3}{2} h_x^2\right) \mathrm{d}x + \int_0^{x_m} \gamma_{sl} \left(1 + \frac{1}{2} h_x^2\right) \mathrm{d}x + \int_{x_m}^{x_e} \gamma_{sv} \left(1 + \frac{1}{2} h_x^2\right) \mathrm{d}x + \gamma R \left(\frac{\pi}{2} - h_x(x_m) - \theta_b\right), \tag{A 1}$$

where γ_{sl}, γ_{sv}, and γ denote the solid–liquid, solid–vapour, and liquid–vapour surface energies respectively, and $x = x_e$ is the horizontal position of the end of the beam. Note that in writing down the above energy, we have linearized for small slope $h_x \ll 1$ but kept the quadratic term in the expressions for the surface energies as these will give rise to linear terms upon using a variational principle. Furthermore, for simplicity we assume that the equilibrium contact angle on a rigid surface $\theta_e = 0$, so that $\gamma_{sv} - \gamma_{sl} = \gamma$, but allow the contact angle on the beam, θ_b, to vary. Finally, the radius of curvature of the meniscus $R = h(x_m)/[\cos\theta_b - h_x(x_m)\sin\theta_b]$. We consider only the case of separated ends, but note that the calculation for the touching and sticking end configurations will follow a similar pattern.

We wish to minimize this energy subject to the constraints of constant volume of liquid and inextensibility of the beam. We therefore consider the functional

$$I(h) = E(h) + \lambda \left[\frac{v}{2} - \int_0^{x_m} h \,\mathrm{d}x + R^2 \left(\frac{\pi}{4} - h_x(x_m) - \theta_b\right)\right] + \mu \left[l - \int_0^{x_e} \left(1 + \frac{1}{2} h_x^2\right) \mathrm{d}x\right], \tag{A 2}$$

where λ and μ are Lagrange multipliers, and we have assumed that $\theta_b \ll 1$ to simplify the expression for the meniscus volume. We consider a small perturbation $\zeta_i \mapsto \zeta_i + \delta\zeta_i$ ($\delta \ll 1$) for all variables ζ_i, noting that for a static equilibrium $\delta I/\delta\zeta_i = 0$ for each ζ_i. Integrating by parts twice, keeping only terms linear in θ_b, h_x, and requiring the variation to vanish at the extremum, we have

$$\frac{\delta I}{\delta x_e} = 0 \Rightarrow \mu = \gamma_{sv}, \tag{A 3a}$$

$$\frac{\delta I}{\delta \theta_b} = 0 \Rightarrow \lambda = -\frac{\gamma}{h(x_m)}, \tag{A 3b}$$

$$\frac{\delta I}{\delta h_x(x_m)} = 0 \Rightarrow \left[\frac{\partial^2 h}{\partial x^2}\right]_-^+ = 0, \tag{A 3c}$$

$$\frac{\delta I}{\delta h(x_m)} = 0 \Rightarrow \left[\frac{\partial^3 h}{\partial x^3}\right]_-^+ = -\frac{\gamma}{B}\theta_b, \tag{A 3d}$$

$$\frac{\delta I}{\delta x_m} = 0 \Rightarrow \theta_b = -\frac{1}{2}h_x(x_m), \tag{A 3e}$$

where we have used the appropriate boundary conditions at $x = 0$ and $x = x_e$. We note that (A 3*b*) identifies the Lagrange multiplier λ as the capillary pressure within the liquid. Finally, setting $\delta I/\delta h = 0$ leads to

$$Bh''''(x) = \begin{cases} -\gamma\left[h''(x) + \dfrac{1}{h(x_m)}\right], & 0 < x < x_m, \\ 0, & x_m < x < \ell, \end{cases} \tag{A 4}$$

in agreement with (2.1) for $\theta_e = 0$. It is interesting to note from (A 3*e*) that the contact angle θ_b is not equal to $\theta_e = 0$, but changes slightly to take into account the bending of the beam (Shanahan 1985). However, we note that once (A 3*d*) is non-dimensionalized using the elastocapillary length $\ell_{ec} = (B/\gamma)^{1/2}$, the right-hand side is at most w/ℓ; the neglect of this term is thus entirely consistent with neglecting the tension in the beam, as discussed in § 2.3. We have for clarity of presentation therefore assumed $\theta_b = \theta_e$ in the main text.

Appendix B. Numerical solution of evolution equations

As noted in § 2.4, we solve the partial differential equation (2.21) by mapping the moving domain $X \in [0, X_m(T)]$ to $Z \in [0, 1]$. We achieve this by letting $Z = X/X_m(T)$ and using the chain rule

$$\left(\frac{\partial}{\partial T}\right)_X = \left(\frac{\partial}{\partial T}\right)_Z - \frac{\dot{X}_m Z}{X_m}\left(\frac{\partial}{\partial Z}\right)_T, \quad \left(\frac{\partial}{\partial X}\right)_T = \frac{1}{X_m}\left(\frac{\partial}{\partial Z}\right)_T, \tag{B 1}$$

where $\dot{()}$ denotes $\mathrm{d}()/\mathrm{d}T$ and $(\partial/\partial a)_b$ denotes partial differentiation with respect to a whilst holding b fixed. We see that this transformation of variables introduces an additional advective term to (2.21). We also introduce the quantity

$$U(Z, T) = H(Z, T)X_m(T) \tag{B 2}$$

so that the governing equation (2.21) may be rewritten in the form

$$\frac{\partial U}{\partial T} + \frac{\partial Q}{\partial Z} = 0, \tag{B 3}$$

with Q representing a horizontal flux.

We discretize the spatial domain into $N + 1$ cells of equal width ΔZ, where the approximate value of U in the jth cell, denoted U_j, is evaluated at the mid-point of the cell, while the fluxes $Q_{j\pm1/2}$ are evaluated at the end-points. Spatial discretization of (B 3) using central finite differences then leads to a set of ordinary differential equations

$$\frac{\mathrm{d}U_j}{\mathrm{d}T} = -\frac{1}{\Delta Z}(Q_{j+1/2} - Q_{j-1/2}), \quad j = 1, 2, \ldots, N. \tag{B 4}$$

together with

$$\frac{\mathrm{d}X_m}{\mathrm{d}T} = -\frac{[U^2 U_{ZZZZZ}]_{N+1/2}}{3X_m^8}, \tag{B 5}$$

Current regime	Event	New regime
I	$H(L) \leqslant 0$	II
II	$H(L) > 0$	I
II	$H_X(X_m) \geqslant 0$	III
III	$X_c > L$	II
I–III	$X_m > L$	Stop

TABLE 1. Event functions used to change regime in the dynamic model.

while the remaining six boundary conditions are applied through the addition of three ghost points on either side of the boundary. The system of ordinary differential equations (B 4)–(B 5) is solved using MATLAB's stiff solver `ode15s`, with the Jacobian being calculated using complex step differentiation (using the algorithm detailed by Shampine 2007) and full advantage being taken of the sparsity of the system.

Finally, we must take care to ensure that we are using the correct boundary conditions for the ends of the beam, i.e. that the beam is in the correct regime. This is done using event functions as outlined in table 1 (for clarity these are written in terms of the original variables), with the boundary conditions at $Z = 1$ changed appropriately. In particular, we note that the computation was stopped if the meniscus reached the end of the beam.

REFERENCES

ANDREOTTI, B., MARCHAND, A., DAS, S. & SNOEIJER, J. H. 2011 Elastocapillary instability under partial wetting conditions: bending versus buckling. *Phys. Rev.* E **84**, 061601.

ARISTOFF, J. M., DUPRAT, C. & STONE, H. A. 2011 Elastocapillary imbibition. *Intl J. Non Linear Mech.* **46** (4), 648–656.

BERKOWSKI, K. L., PLUNKETT, K. N., YU, Q. & MOORE, J. S. 2005 Introduction to photolithography: preparation of microscale polymer silhouettes. *J. Chem. Ed.* **82**, 1365–1369.

BICO, J., ROMAN, B., MOULIN, L. & BOUDAOUD, A. 2004 Elastocapillary coalescence in wet hair. *Nature* **432**, 690.

BOUDAOUD, A., BICO, J. & ROMAN, B. 2007 Elastocapillary coalescence: aggregation and fragmentation with a maximal size. *Phys. Rev.* E **76**, 060102(R).

CHANDRA, D. & YANG, S. 2009 Capillary-force-induced clustering of micropillar arrays: is it caused by isolated capillary bridges or by the lateral capillary meniscus interaction force? *Langmuir* **25** (18), 10430–10434.

CRASTER, R. V. & MATAR, O. K. 2009 Dynamics and stability of thin liquid films. *Rev. Mod. Phys.* **81**, 1131–1198.

DAS, S., MARCHAND, A., ANDREOTTI, B. & SNOEIJER, J. H. 2011 Elastic deformation due to tangential capillary forces. *Phys. Fluids* **23**, 072006.

DELAMARCHE, E., SCHMID, H., MICHEL, B. & BIEBUYCK, H. 1997 Stability of molded polydimethylsiloxane microstructures. *Adv. Mater.* **9**, 741–746.

DUPRAT, C., ARISTOFF, J. M. & STONE, H. A. 2011 Dynamics of elastocapillary rise. *J. Fluid Mech.* **679**, 641–654.

FARSHID CHINI, S. & AMIRFAZLI, A. 2010 Understanding pattern collapse in photolithography process due to capillary forces. *Langmuir* **26** (16), 13707–13714.

DE GENNES, P.-G., BROCHARD-WYART, F. & QUÉRÉ, D. 2003 *Capillarity and Wetting Phenomena: Drops, Bubbles, Pearls, Waves*. Springer.

GROTBERG, J. B. & JENSEN, O. E. 2004 Biofluid mechanics in flexible tubes. *Annu. Rev. Fluid Mech.* **36**, 121–147.

HALPERN, D. & GROTBERG, J. B. 1992 Fluid-elastic instabilities of liquid-lined flexible tubes. *J. Fluid Mech.* **244**, 615–632.

VAN HONSCHOTEN, J. W., ESCALANTE, M., TAS, N. R., JANSEN, H. V. & ELWENSPOEK, M. 2007 Elastocapillary filling of deformable nanochannels. *J. Appl. Phys.* **101**, 094310.

HUANG, J., JUSZKIEWICZ, M., DE JEU, W. H., CERDA, E., EMRICK, T., MENON, N. & RUSSELL, T. P. 2007 Capillary wrinkling of floating thin polymer films. *Science* **317**, 650–653.

HURE, J., ROMAN, B. & BICO, J. 2011 Wrapping an adhesive sphere with an elastic sheet. *Phys. Rev. Lett.* **106**, 174301.

JENSEN, O. E. 1997 The thin liquid lining of a weakly curved cylindrical tube. *J. Fluid Mech.* **331**, 373–403.

KIM, H.-Y. & MAHADEVAN, L. 2006 Capillary rise between elastic sheets. *J. Fluid Mech.* **548**, 141–150.

KWON, H.-M., KIM, H.-Y., PUELL, J. & MAHADEVAN, L. 2008 Equilibrium of an elastically confined liquid drop. *J. Appl. Phys.* **103**, 093519.

LANDAU, L. D. & LIFSCHITZ, E. M. 1959 *Theory of Elasticity*. Pergamon.

LEAL, L. G. 2007 *Advanced Transport Phenomena*. Cambridge University Press.

LEE, H.-J., PARK, J.-T., YOO, J., AN, I. & OH, H.-K. 2002 Resist pattern collapse with top rounding resist profile. *Japan J. Appl. Phys.* **42**, 3922–3927.

MAJIDI, C. 2007 Remarks on formulating an adhesion problem using Euler's elastica. *Mech. Res. Commun.* **34**, 85–90.

MANSFIELD, E. H., SEPANGI, H. R. & EASTWOOD, E. A. 1997 Equilibrium and mutual attraction or repulsion of objects supported by surface tension. *Phil. Trans. R. Soc. Lond.* A **355**, 869–919.

MARCHAND, A., DAS, S., SNOEIJER, J. H. & ANDREOTTI, B. 2012 Capillary pressure and contact line force on a soft solid. *Phys. Rev. Lett.* **108**, 094301.

MASTRANGELO, C. H & HSU, H. 1993*a* Mechanical stability and adhesion of microstructures under capillary forces. Part 1. Basic theory. *J. Microelectromech. Syst.* **2**, 33–43.

MASTRANGELO, C. H & HSU, H. 1993*b* Mechanical stability and adhesion of microstructures under capillary forces. Part 2. Experiments. *J. Microelectromech. Syst.* **2**, 44–55.

MATAR, O. K. & KUMAR, S. 2004 Rupture of a surfactant-covered thin liquid film on a flexible wall. *SIAM J. Appl. Math.* **64**, 2144–2166.

POKROY, B., KANG, S. G., MAHADEVAN, L. & AIZENBERG, J. 2009 Self-organization of a mesoscale bristle into ordered, hierarchical helical assemblies. *Science* **323**, 237–240.

PY, C., REVERDY, P., DOPPLER, L., BICO, J., ROMAN, B. & BAROUD, C. N. 2007 Capillary origami: spontaneous wrapping of a droplet with an elastic sheet. *Phys. Rev. Lett.* **98**, 156103.

RACCURT, O., TARDIF, F., ARNAUD D'AVITAYA, F. & VAREINE, T. 2004 Influence of liquid surface tension on stiction of SOI MEMS. *J. Micromech. Microengng* **14**, 1083–1090.

ROMAN, B. & BICO, J. 2010 Elasto-capillarity: deforming an elastic structure with a liquid droplet. *J. Phys.: Condens Mater* **22**, 493101.

ROY, R. V. & SCHWARTZ, L. W. 1999 On the stability of liquid ridges. *J. Fluid Mech.* **391**, 293–318.

SHAMPINE, L. F. 2007 Accurate numerical derivatives in MATLAB. *ACM Trans. Math. Softw.* **33**, 26.

SHANAHAN, M. E. R. 1985 Contact angle equilibrium on thin elastic solids. *J. Adhes.* **18**, 247–267.

VAN SPENGEN, W. M., PUERS, R. & DE WOLF, I. 2002 A physical model to predict stiction in MEMS. *J. Micromech. Microengng* **12**, 702–713.

TANAKA, T., MORIGAMI, M. & ATODA, N. 1993 Mechanism of resist pattern collapse during development process. *Japan J. Appl. Phys.* **31**, 6059–6064.

VELLA, D., ADDA-BEDIA, M. & CERDA, E. 2010 Capillary wrinkling of elastic membranes. *Soft Matt.* **6**, 5778–5782.

WEINSTEIN, S. J., DUSSAN, V. E. B. & UNGAR, L. H. 1990 A theoretical study of two-phase flow through a narrow gap with a moving contact line: viscous fingering in a Hele-Shaw cell. *J. Fluid Mech.* **221**, 53–76.

XIA, Y. & WHITESIDES, G. M. 1998 Soft lithography. *Annu. Rev. Mater. Sci.* **28**, 153–184.

YOUNG, T. 1805 An essay on the cohesion of fluids. *Phil. Trans. R. Soc. Lond.* **95**, 65–87.